frontiers in Electronic Materials

ORIGINAL RESEARCH
published: 02 March 2022
doi: 10.3389/femat.2022.851294

Phenalene—A New Ring-Locked Vinyl Bridge for Nonfullerene Acceptors With Enhanced Chemical and Photochemical Stabilities

Hongtao Liu[1†], *Cheng-Tien Hsieh*[2†], *Yaxin He*[1], *Chu-Chen Chueh*[2*] *and Zhong'an Li*[1*]

[1]*Key Laboratory for Material Chemistry of Energy Conversion and Storage Ministry of Education, School of Chemistry and Chemical Engineering, Huazhong University of Science and Technology, Wuhan, China,* [2]*Department of Chemical Engineering and Advanced Research Center for Green Materials Science and Technology, National Taiwan University, Taipei, Taiwan*

Currently, the two exocyclic vinyl bridges in the acceptor–donor–acceptor (A–D–A)-type nonfullerene acceptors (NFAs) have been widely recognized as one of the most vulnerable sites under external stresses. Embedding the exocyclic vinyl bridges into an aromatic ring could be a feasible solution to stabilize them. Herein, we successfully develop a phenalene-locked vinyl bridge via a titanium tetrachloride—pyridine catalytic Knoevenagel condensation, to synthesize two new A–D–A-type unfused NFAs, EH-FPCN and O-CPCN, wherein malononitrile is used as the electron-deficient terminal group while fluorene and carbazole rings are used as the electron-rich cores, respectively. These two NFAs possess wide bandgaps associated with deep energy levels, and significantly enhanced chemical and photochemical stabilities compared to the analogue molecule O-CzCN with normal exocyclic vinyl bridges. When pairing with a narrow bandgap polymer donor PTB7-Th, the fabricated EH-FPCN- and O-CPCN-based organic solar cells achieved power conversion efficiencies of 0.91 and 1.62%, respectively. The higher efficiencies for O-CPCN is attributed to its better film morphology and higher electron mobility in the blend film. Overall, this work provides a new design strategy to stabilize the vulnerable vinyl bridges of A–D–A-type NFAs.

Keywords: organic solar cells, non-fullerene acceptors, chemical and photochemical stabilities, ring-locking strategy, phenalene-locked vinyl bridge

OPEN ACCESS

Edited by:
Aung Ko Ko Kyaw,
Southern University of Science and Technology, China

Reviewed by:
Zuo-Quan Jiang,
Soochow University, China
Jingde Chen,
Soochow University, China

***Correspondence:**
Chu-Chen Chueh
cchueh@ntu.edu.tw
Zhong'an Li
lizha@hust.edu.cn

†These authors have contributed equally to this work

Specialty section:
This article was submitted to Optoelectronic Materials, a section of the journal Frontiers in Electronic Materials

Received: *09 January 2022*
Accepted: *07 February 2022*
Published: *02 March 2022*

Citation:
Liu H, Hsieh C-T, He Y, Chueh C-C and Li Z (2022) Phenalene—A New Ring-Locked Vinyl Bridge for Nonfullerene Acceptors With Enhanced Chemical and Photochemical Stabilities. Front. Electron. Mater. 2:851294. doi: 10.3389/femat.2022.851294

INTRODUCTION

As one of the third-generation photovoltaic techniques, organic solar cells (OSCs) have demonstrated outstanding potentials in the fields of flexible devices, semi-transparent devices, indoor photovoltaics, and so on (Liu et al., 2021c; Dauzon et al., 2021; Kini et al., 2021; Xie et al., 2021). Excitingly, the record power conversion efficiency (PCE) of OSCs has been continuously rising in recent years, and a value exceeding 19% has been achieved already (Cui et al., 2021; Wang et al., 2021), attributed to the innovative design and exploitation of photovoltaic materials and device architecture (Li et al., 2019; Cui and Li, 2021; Liu W. et al., 2021; Gao et al., 2021; Ren et al., 2021; Yin et al., 2021; Zheng et al., 2021). In particular, A–D–A-type nonfullerene acceptors (NFAs) play the most critical role in achieving high-performance OSCs since the emergence of the representative NFA molecule, namely ITIC, reported by Zhan et al., in 2015 (Lin et al., 2015), where "D" and "A" represent the electron-donating and electron-accepting units, respectively. Currently, most of ITIC-

like NFAs are constructed by using a largely fused ring as the D core such as indacenodithieno[3,2-b]thiophene (IDTT) end-capped by 2 A units such as 2-(3-oxo-2,3-dihydroinden-1-ylidene)malononitrile (INCN). However, such design always involves high synthetic complexity, thereby limiting their further practical applications. In this context, many researchers have paid attention to explore new A–D–A-type NFAs with semi-fused (Li et al., 2018; Huang et al., 2019; Liu X. et al., 2020; Luo et al., 2021) and even fully unfused electron-rich cores (Bi et al., 2021; Ma et al., 2021; Wen et al., 2021; Zhou et al., 2021).

In addition to simplifying the materials synthesis, improving the stability is another critical factor for NFAs to be commercialized. From the structure point of view, A–D–A-type NFAs always contain two exocyclic vinyl groups as the conjugation bridges between D and A units as a result of the condensation reaction. Although the vinyl bridges improve the planarity and enlarge conjugation length, leading to a smaller bandgap and enhanced charge transport properties, they encounter unsatisfactory intrinsic chemical and photochemical stabilities due to the strong push-pull effect that makes them very electrophilic (Li W. et al., 2021; Liu et al., 2021a). In this regard, the nucleophiles such as primary and secondary amines in the commonly used cathode interfacial materials (PEI and PEIE) would easily engender Michael addition reactions with the β-carbon atoms of these electrophilic vinyl bridges (Hu et al., 2018; Zeng et al., 2021). In the meanwhile, photooxidation and/or photodegradation of vinyl bridges also occur easily due to the generation of reactive oxygen species (ROS) under light irradiation (Guo et al., 2019; Jiang et al., 2019; Park and Son, 2019; Liu B. et al., 2020). To improve the chemical and photochemical stabilities of NFAs, scientists have proposed interfacial engineering approaches. For example, protonation of PEIE (Xiong et al., 2019) or formation of Zn^{2+}-chelated PEI (Qin et al., 2020) has shown to significantly reduce its reactivity with the NFAs as reported by Zhou et al. More recently, Forrest et al. improved the chemical and morphological stabilities at organic active layer/inorganic interfacial layers by inserting buffer layers between them (Li Y. et al., 2021). Besides, development of new interfacial and charge transport materials with low reactivity and/or low defects (Cui et al., 2020; Kyeong et al., 2021; Prasetio et al., 2021) as well as additive engineering such as doping a stabilizer to scavenge ROS (Qin et al., 2017; Du et al., 2019; Lu et al., 2021) have also been used as alternative approaches.

Despite these successes, it would be of greater importance to develop efficient molecular strategies that can improve the intrinsic stability of NFAs at the molecular level; however, the related progress remains tardy. For example, Li et al. have demonstrated that the undesired photoisomerization of vinyl bridges of NFAs can be effectively suppressed by enhancing the intermolecular packing via the subtle side-chain modification (Yu et al., 2019; Liu Z.-X. et al., 2021). Moreover, construction of all-fused NFAs is also a feasible design strategy for enhancing the stability of NFAs (Zhu et al., 2021). Recently, we reported a new ring-locked strategy by incorporating the vinyl bridge of NFAs into a cyclohexane ring, which significantly improves the chemical and photochemical stabilities of vinyl bridges due to enhanced steric hindrance of nucleophilic attaching and suppressed photoisomerization induced by the noncovalent interactions (Liu et al., 2021b). Therefore, it would be reasonable to embed the exocyclic vinyl bridges into an aromatic ring for enhancing their stabilities.

Phenalene fused by three benzenes arranging in a triangle has a simple and symmetrical molecular structure. Since Haddon pointed out the potential of phenalene to construct molecular conductors in 1975 (Haddon, 1975), researchers have designed and synthesized lots of phenalene-based materials for broad applications such as organic electronics, energy storage, information processing system, etc (Mandal et al., 2005; Morita et al., 2011; Raman et al., 2013). Herein, based on our ring-locked strategy, we successfully develop a feasible synthetic route to embed the exocyclic vinyl bridges into the phenalene unit as a conjugation bridge of A–D–A-type NFAs (**Figure 1A**). To reduce the synthetic complexity, carbazole and fluorene are used as the central core for constructing phenalene-locked NFAs with an unfused structure, EH-FPCN and O-CPCN (**Figure 1B**), respectively. Both of them show good thermal/chemical/photochemical stabilities, broadened and red-shifted absorption, and decreased lowest unoccupied molecular orbital (LUMO) energy levels compared to the reference O-CzCN (**Figure 1B**) without a phenalene bridge. When pairing with a polymer donor PTB7-Th, the resulting EH-FPCN- and O-CPCN-based OSCs can achieve PCEs of 0.91 and 1.62%, respectively. The better performance of O-CPCN is attributed to its enhanced electron mobility and more uniform blend film morphology.

RESULTS AND DISCUSSION

Synthesis and Structural Characterization

Scheme 1 displays the synthetic route of the targeting molecules.1-Oxo-1H-phenalen-3-yl trifluoromethanesulfonate (OTf-P) was synthesized according to the literature method (Ospina et al., 2017). By employing an unusual titanium tetrachloride–pyridine catalytic system (Liu et al., 2021b), the cyano-substituted phenalene unit (OTf-PCN) was obtained *via* a Knoevenagel condensation between OTf-P and malononitrile. Then, OTf-PCN reacted with fluorene and carbazole borate esters such as EH-Fl-Bpin and O-Cz-Bpin to produce EH-FPCN and O-CPCN via a Pd-catalyzed Suzuki coupling, respectively. Finally, O-CzCN as the control molecule without the ring-locked bridge was synthesized based on the trimethylamine-catalyzed Knoevenagel condensation between O-CzCHO (**Supplementary Scheme S1**) and malononitrile. The detailed syntheses and structural characterizations are provided in the Supporting Information.

Thermal Properties

The thermal properties of NFAs were studied by thermogravimetric analysis (TGA) and differential scanning calorimetry (DSC) in nitrogen. As shown in **Supplementary**

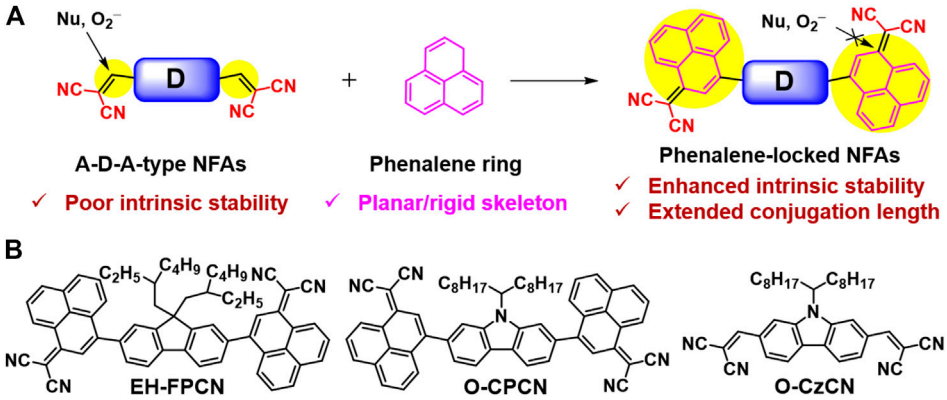

FIGURE 1 | (A) Illustration of design strategy of phenalene-locked A–D–A-type NFAs; **(B)** Chemical structures of O-CzCN, EH-FPCN, and O-CPCN.

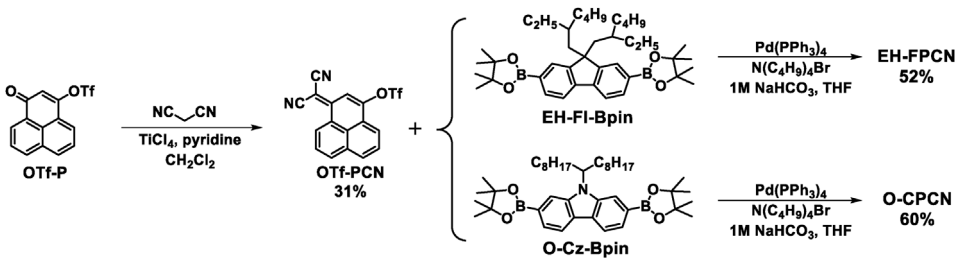

SCHEME 1 | Synthetic routes of EH-FPCN and O-CPCN.

TABLE 1 | Optical and electrochemical data of NFAs.

NFAs	ε_{max}[a] (10^4 M^{-1} cm^{-1})	λ_{sol}[b] (nm)	λ_{fil}[c] (nm)	$E_{g,opt}$[d] (eV)	E_{HOMO}[e] (eV)	E_{LUMO}[e] (eV)	$E_{g,ec}$[f] (eV)
EH-FPCN	3.8 (487 nm)	440, 487	452, 497	1.99	−5.91	−3.60	2.31
O-CPCN	3.1 (488 nm)	448, 488	463, 484	1.95	−5.73	−3.62	2.11
O-CzCN	7.0 (412 nm)	412	363, 393, 457	2.37	−5.95	−3.52	2.43

[a] *Molar extinction coefficients measured in 10^{-5} M CF, solutions. The strong absorption peaks of acceptors*[b] *in CF, and*[c] *as thin films.*[d] *Calculated from the film absorption edge (λ_{edge}) according to the equation $E_{g,opt} = 1{,}240/\lambda_{edge}$.*[e] *Measured by CVs, of acceptors in dichloromethane/0.1 M Bu_4NPF_6 solution. Calculated according to the equation $E_{HOMO/LUMO} = -(E_{ox/red} + 4.80)$ eV.*[f] *Calculated according to the equation $E_{g,ec} = E_{LUMO} - E_{HOMO}$.*

Figure S1A, the thermal decomposition temperatures for EH-FPCN, O-CPCN, and O-CzCN, corresponding to 5% weight loss, were estimated to be 389, 396, and 340°C, respectively. This result clearly shows that the introduction of phenalene-locked bridge improves the thermal stability of resulting NFAs. Notably, there is no glass transition temperature (T_g) found for all molecules (**Supplementary Figure S1B**). Both EH-FPCN and O-CzCN exhibit an amorphous nature because no endothermic and exothermic peaks are observed in both heating and cooling processes. Differently, O-CPCN possesses an obvious endothermic peak at 217°C in the heating process assigned as the melting point, but no exothermic peak is found in the cooling process. This phenomenon could be attributed to the effect of alkyl chains on the molecular stacking. As compared to the branched alkyl chains, the linear alkyl chains are conducive to enhance intermolecular stacking (Holliday et al., 2016).

Photophysical and Electrochemical Properties

Figures 2A,B show the UV–Vis absorption spectra of EH-FPCN, O-CPCN, and O-CzCN, and the corresponding data are summarized in **Table 1**. In the chloroform (CF) solutions (**Figure 2A**), EH-FPCN and O-CPCN exhibit broadened and bathochromic-shifted absorption bands in comparison with that of O-CzCN due to the extended conjugation. However, the molar extinction coefficients (ε_{max}s) of these phenalene-locked NFAs are decreased to 3.0–4.0 × 10^4 M^{-1} cm^{-1} when comparing that of O-CzCN (7.0 × 10^4 M^{-1} cm^{-1}). This is possibly due to their

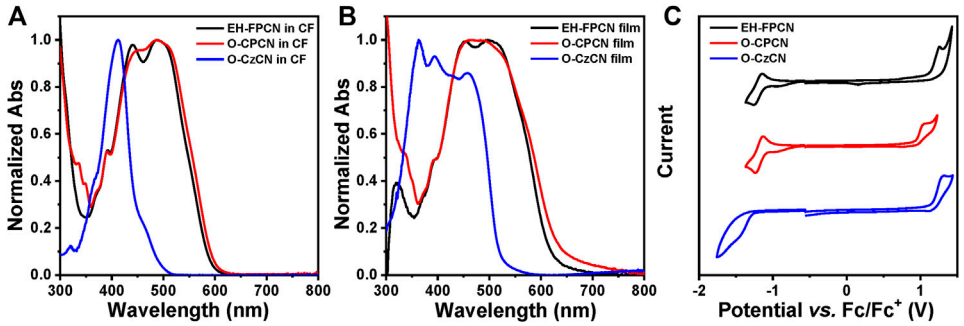

FIGURE 2 | Normalized UV–Vis absorption spectra of EH-FPCN, O-CPCN, and O-CzCN **(A)** in chloroform and **(B)** as thin films; **(C)** CVs of EH-FPCN, O-CPCN, and O-CzCN in dichloromethane/0.1 M Bu_4NPF_6.

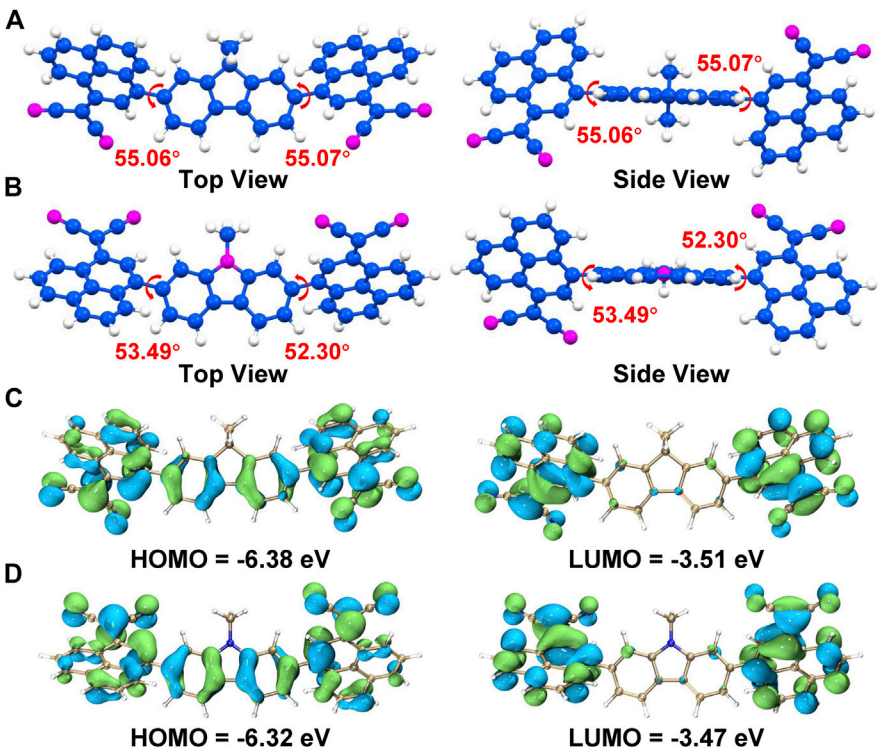

FIGURE 3 | The DFT-optimized geometrical structures of **(A)** EH-FPCN and **(B)** O-CPCN, the hydrogen atoms are marked in white, carbon atoms in blue, and nitrogen atoms in magenta; The DFT-calculated electron distributions of Frontier molecular orbitals of **(C)** EHFPCN and **(D)** O-CPCN.

nonplanar molecular conformations (See 2.4 Theory Calculations). Compared with the solution absorption, the enhanced intermolecular interactions in the solid-state make both film absorption bands of EH-FPCN and O-CPCN more broadened with a red-shift of ~10 nm (**Figure 2B**). The long wavelength tail for O-CPCN may be due to the enhanced energy disorder. Note that the O-CzCN film possesses both hypsochromic-shifted and bathochromic-shifted absorption peaks, indicating the possible formation of both H- and J-aggregations (Yassin et al., 2011). Comparison of the above results thus suggests the introduction of phenalene-locked bridge can suppress the H-aggregation of NFAs in solid state. The optical bandgaps (E_g) values for EH-FPCN, O-CPCN, and O-CzCN estimated from the film absorption edge are 1.99, 1.95, and 2.37 eV, respectively. The smaller E_g value for O-CPCN than EH-FPCN is due to the enhanced electron-donating ability of carbazole.

The electrochemical properties of these acceptors were investigated by cyclic voltammetry (CV) in a dichloromethane solution containing

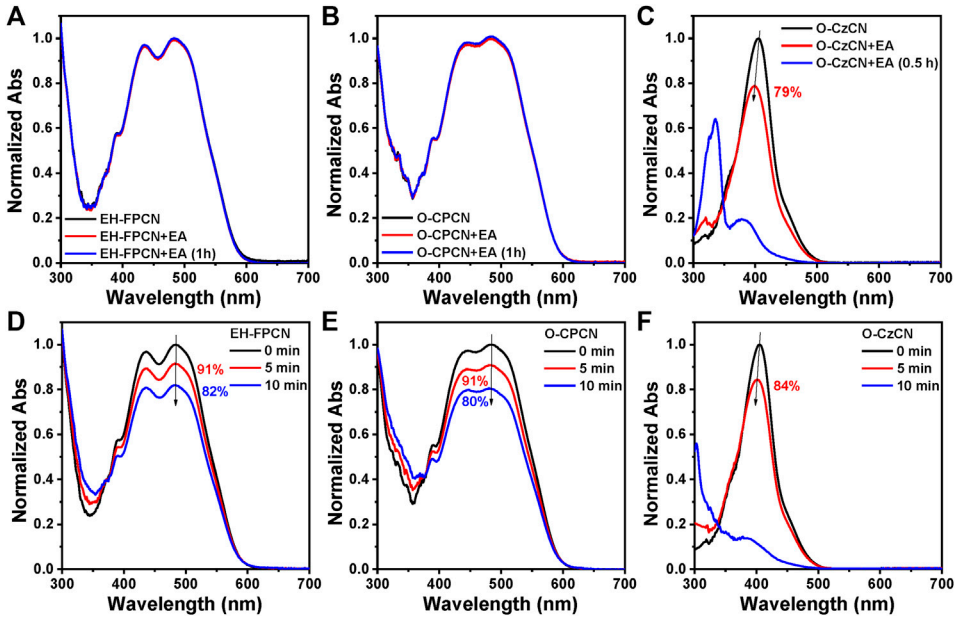

FIGURE 4 | Normalized UV–Vis absorption spectra of NFAs: **(A)** EH-FPCN, **(B)** O-CPCN and **(C)** O-CzCN before and after adding EA in THF:H_2O mixtures (96:4, V/V). The concentration of NFAs is 1×10^{-5} M, while that of EA is 1×10^{-3} M. Normalized UV–Vis absorption spectra of NFAs in THF in air under different irradiation time: **(D)** EH-FPCN, **(E)** O-CPCN, and **(F)** O-CzCN. The concentration of NFAs is 1×10^{-5} M, and the light intensity is 100 mW cm^{-2}.

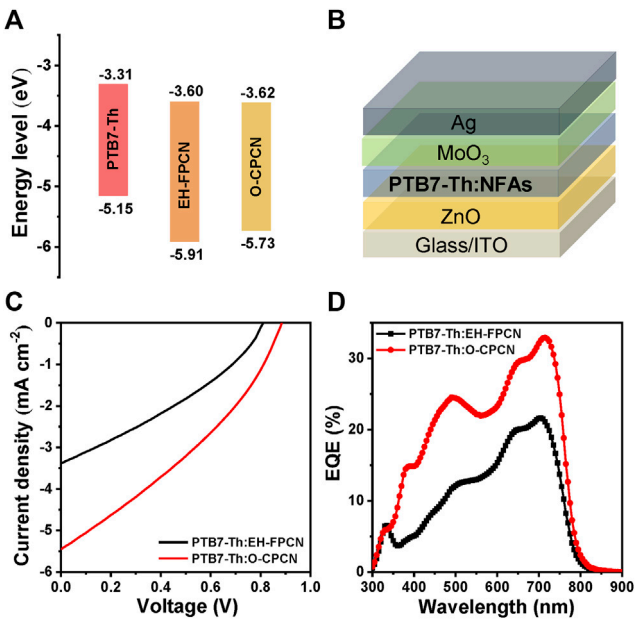

FIGURE 5 | (A) Energy levels of PTB7-Th, EH-FPCN, and O-CPCN; **(B)** Inverted OSC architecture; **(C)** *J–V* curves of PTB7-Th:NFAs-based devices; **(D)** EQE curves of PTB7-Th:NFAs-based devices.

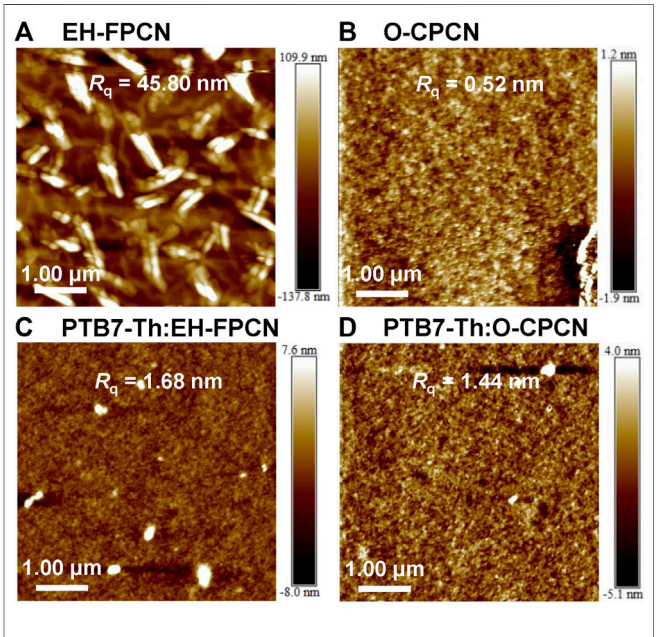

FIGURE 6 | The AFM images (5.00 × 5.00 μm) of films: **(A)** EH-FPCN, **(B)** O-CPCN, **(C)** PTB7-Th:EH-FPCN, and **(D)** PTB7-Th:O-CPCN.

0.1 mol L^{-1} of Bu_4NPF_6. As shown in **Figure 2C** and **Table 1**, both EH-FPCN and O-CPCN have a quasi-reversible redox peak in the reduction process and an irreversible redox peak in the oxidation process. Compared to the reference O-CzCN, the introduction of phenalene-bridge in O-CPCN elevates the HOMO energy level and decreases the LUMO energy level. Moreover, replacing carbazole with fluorene unit induces a decreased HOMO level by ~0.2 eV, associated with a slight change on the LUMO level.

TABLE 2 | The optimal photovoltaic parameters of OSCs based on PTB7-Th:NFAs.

Donor:Acceptor	V_{oc} (V)	J_{sc} (mA cm^{-2})	FF (%)	PCE (%)
PTB7-Th:EH-FPCN	0.77 ± 0.04	3.33 ± 0.04	32.99 ± 0.28	0.85 ± 0.06 (0.91)
PTB7-Th:O-CPCN	0.88 ± 0.01	5.42 ± 0.03	33.30 ± 0.20	1.59 ± 0.03 (1.62)

Data obtained from the average of 15 individual devices, and the best PCEs, are shown in brackets.

Theory Calculations

To investigate the molecular conformation of EH-FPCN and O-CPCN, the density functional theory (DFT) calculations were conducted, which show that both NFAs have over 50° dihedral angles between the phenalene and fluorene/carbazole cores, as shown in **Figures 3A,B**. Such nonplanar molecular conformation may cause poor molecular stacking and thus weaken the intra-/intermolecular charge transfer. **Figures 3C,D** present the electron distribution of Frontier molecular orbitals of EH-FPCN and O-CPCN performed at the B3LYP/6-31G(d) level of theory. It is clearly shown that the wave function of HOMO delocalizes on the whole conjugated skeleton, and the wave function of LUMO mainly delocalizes on the phenalene–malononitrile units. The overlap between the wave function of HOMO and LUMO is favorable to exciton generation and charge transfer (Krishna et al., 2014).

Chemical and Photochemical Stabilities

The effects of phenalene-locked bridge on the chemical stability of three NFAs were then studied by testing the solution absorption change with or without adding a strong nucleophile (ethanol amine, EA) under different time. **Figures 4A,B** show that the absorption spectra have no significant changes after adding 100 equiv. molar amount of EA into the 1×10^{-5} M EH-FPCN and O-CPCN solutions for 1 h. In sharp contrast, under the same conditions, the absorption intensity of O-CzCN solution immediately decreased by 21% after adding EA, and further decreased by more than 80% after 0.5 h, as shown in **Figure 4C**. The photochemical stability was then investigated by monitoring the solution absorption change under different light irradiation time (Xenon lamp, 100 mW cm^{-2}). After light irradiation for 10 min, the absorption intensities of EH-FPCN and O-CPCN only decreased by ~18 and ~20%, respectively (**Figures 4D,E**), while that of O-CzCN exhibited a 16% decrease only after light irradiation for 5 min (**Figure 4F**), followed by a complete degradation after 10 min. These results therefore strongly illustrate that the phenalene-locked strategy can effectively enhance the chemical and photochemical stabilities of A–D–A-type NFAs by reducing the reactivity of vinyl bridges. Moreover, the film photostabilities of phenalene-locked NFAs were also measured under light irradiation (**Supplementary Figure S2**). After 2 h of continuous irradiation, the maximum absorption peak intensity of O-CPCN film retained 73% of its initial value, while only 34% was found for the EH-FPCN film, which could be attributed to the poor antioxidative ability of fluorene core in EH-FPCN.

Photovoltaic Performance

To investigate the photovoltaic performance of EH-FPCN and O-CPCN, a representative low-bandgap polymer, PTB7-Th, was chosen as the donor to form a bulk heterojunction (BHJ) blend due to the compatible energy levels (**Figure 5A**) and bandgaps (**Supplementary Figure S3**), and the donor:NFA weight ratio is optimized to 1:0.8. The devices were fabricated based on an inverted architecture: ITO/ZnO/PTB7-Th:NFAs/MoO_3/Ag (**Figure 5B**). The resultant current density–voltage (J–V) curves are shown in **Figure 5C** and the photovoltaic parameters summarized in **Table 2**. As shown, the optimal PCEs for EH-FPCN and O-CPCN-based devices are 0.91 and 1.62%, respectively. The low PCEs may be attributed to the inferior exciton diffusion and separation efficiencies, which caused by the poor molecular planarity of phenalene-locked acceptors and the weak electron-withdrawing ability of malononitrile. This thus suggests that more structural optimizations need to be done for the phenalene-locked NFAs. Compared to the EH-FPCN-based device, the higher PCE for the O-CPCN-based device is benefited from its enhanced open-circuit voltage (V_{oc}) and short-circuit current density (J_{sc}). The external quantum efficiency (EQE) curves (**Figure 5D**) confirm the stronger light response for the O-CPCN-based device, thereby agreeing with the enhanced J_{sc}.

Film Morphology and Electron Mobility

Atomic force microscope (AFM) was then conducted to probe the surface morphology of pristine and blended films. **Figures 6A,B** show the AFM images of pristine EH-FPCN and O-CPCN films, respectively. EH-FPCN has a rough and inhomogeneous morphology with a high root mean square roughness (R_q) of 45.80 nm, indicating its poor film-forming property. In contrary, O-CPCN has a smooth morphology with a low R_q of 0.52 nm. Nonetheless, both NFAs exhibit good compatibility with the PTB7-Th donor, and no phase separation is observed for the resulting BHJ films (**Figures 6C,D**). Moreover, the PTB7-Th:O-CPCN film possesses a smother surface morphology with a lower R_q of 1.44 nm, which is conducive to exciton separation and charge transfer. The electron mobility (μ_e) of active layers were also measured by the space-charge limited current (SCLC) method (**Supplementary Figure S4**) and the calculated μ_e for the EH-FPCN blend (1.01×10^{-3} cm^2 V^{-1} s^{-1}) is lower than that for the O-CPCN blend (3.61×10^{-3} cm^2 V^{-1} s^{-1}). These morphology and electron mobility results thus well explains the superior performance for the PTB7-Th:O-CPCN-based device.

CONCLUSION

In summary, we have successfully developed a phenalene-locked strategy to stabilize the vulnerable vinyl bridges in the A–D–A-type NFAs. As a model design, two phenalene ring-locked unfused NFAs, EH-FPCN and O-CPCN, were synthesized via a facile route, showing enhanced thermal/chemical/photochemical stabilities in comparison with the reference

O-CzCN without phenalene bridge. Moreover, the introduction of phenalene bridge is found to broaden and red-shift the absorption spectra, elevate the HOMO energy levels, and decrease the LUMO energy levels. The nonplanar molecular conformations were observed for both NFAs by DFT calculations, which could negatively affect the ICT process. Due to their wide bandgap feature, a low bandgap polymer donor PTB7-Th was paired to fabricate invert OSCs, and the EH-FPCN- and O-CPCN-based devices achieved PCEs of 0.91 and 1.62%, respectively. SCLC and AFM results suggest that the higher PCE of O-CPCN-based device is benefited from its enhanced electron mobility and smoother BHJ film morphology. Obviously, this work provides a new strategy to enhance the intrinsic stabilities of A–D–A-type NFAs. Further works to improve the photovoltaic performance of phenalene-locked A–D–A-type NFAs still need collaboratively optimize the molecular structures of "D" and "A" units, which is on-going in our lab.

DATA AVAILABILITY STATEMENT

The original contributions presented in the study are included in the article/**Supplementary Material**, further inquiries can be directed to the corresponding author.

AUTHOR CONTRIBUTIONS

HL and ZL: Conceptualization; HL: Investigation, Resources, Data analysis, Writing—original draft; C-TH: Investigation, Data analysis; YH: Resources; C-CC and ZL: Supervision, Funding acquisition, Writing—review and editing.

FUNDING

ZL thanks the financial supports from the Natural Science Foundation of China (No. 22175067), Excellent Youth Foundation of Hubei Scientific Committee (2021CFA065), and the Innovation and Talent Recruitment base of New Energy Chemistry and Device at HUST (No. B2100303). C-CC thanks the financial supports from Top University Project of National Taiwan University (111L7818), and the Ministry of Science and Technology in Taiwan (MOST 109-2628-E-002-008-MY3, 110-2628-E-002-011-).

SUPPLEMENTARY MATERIAL

The Supplementary Material for this article can be found online at: https://www.frontiersin.org/articles/10.3389/femat.2022.851294/full#supplementary-material

REFERENCES

Bi, P., Zhang, S., Ren, J., Chen, Z., Zheng, Z., Cui, Y., et al. (2021). A High-Performance Nonfused Wide-Bandgap Acceptor for Versatile Photovoltaic Applications. *Adv. Mater.* 34, 2108090. doi:10.1002/adma.202108090

Cui, C., and Li, Y. (2021). Morphology Optimization of Photoactive Layers in Organic Solar Cells. *Aggregate* 2 (2), e31. doi:10.1002/agt2.31

Cui, M., Li, D., Du, X., Li, N., Rong, Q., Li, N., et al. (2020). A Cost-Effective, Aqueous-Solution-Processed Cathode Interlayer Based on Organosilica Nanodots for Highly Efficient and Stable Organic Solar Cells. *Adv. Mater.* 32 (38), 2002973. doi:10.1002/adma.202002973

Cui, Y., Xu, Y., Yao, H., Bi, P., Hong, L., Zhang, J., et al. (2021). Single-Junction Organic Photovoltaic Cell with 19% Efficiency. *Adv. Mater.* 33 (41), e2102420. doi:10.1002/adma.202102420

Dauzon, E., Sallenave, X., Plesse, C., Goubard, F., Amassian, A., and Anthopoulos, T. D. (2021). Pushing the Limits of Flexibility and Stretchability of Solar Cells: A Review. *Adv. Mater.* 33 (36), 2101469. doi:10.1002/adma.202101469

Du, X., Lu, X., Zhao, J., Zhang, Y., Li, X., Lin, H., et al. (2019). Hydrogen Bond Induced Green Solvent Processed High Performance Ternary Organic Solar Cells with Good Tolerance on Film Thickness and Blend Ratios. *Adv. Funct. Mater.* 29 (30), 1902078. doi:10.1002/adfm.201902078

Gao, M., Wang, W., Hou, J., and Ye, L. (2021). Control of Aggregated Structure of Photovoltaic Polymers for High-efficiency Solar Cells. *Aggregate* 2 (5), e46. doi:10.1002/agt2.46

Guo, J., Wu, Y., Sun, R., Wang, W., Guo, J., Wu, Q., et al. (2019). Suppressing Photo-Oxidation of Non-fullerene Acceptors and Their Blends in Organic Solar Cells by Exploring Material Design and Employing Friendly Stabilizers. *J. Mater. Chem. A.* 7 (43), 25088–25101. doi:10.1039/c9ta09961a

Haddon, R. (1975). Quantum Chemical Studies in the Design of Organic Metals. III. Odd-Alternant Hydrocarbons - the Phenalenyl (Ply) System. *Aust. J. Chem.* 28 (11), 2343–2351. doi:10.1071/CH9752343

Holliday, S., Ashraf, R. S., Wadsworth, A., Baran, D., Yousaf, S. A., Nielsen, C. B., et al. (2016). High-Efficiency and Air-Stable P3HT-Based Polymer Solar Cells with a New Non-fullerene Acceptor. *Nat. Commun.* 7, 11585. doi:10.1038/ncomms11585

Hu, L., Liu, Y., Mao, L., Xiong, S., Sun, L., Zhao, N., et al. (2018). Chemical Reaction between an ITIC Electron Acceptor and an Amine-Containing Interfacial Layer in Non-fullerene Solar Cells. *J. Mater. Chem. A.* 6 (5), 2273–2278. doi:10.1039/c7ta10306a

Huang, H., Guo, Q., Feng, S., Zhang, C. e., Bi, Z., Xue, W., et al. (2019). Noncovalently Fused-Ring Electron Acceptors with Near-Infrared Absorption for High-Performance Organic Solar Cells. *Nat. Commun.* 10 (1), 3038. doi:10.1038/s41467-019-11001-6

Jiang, Y., Sun, L., Jiang, F., Xie, C., Hu, L., Dong, X., et al. (2019). Photocatalytic Effect of ZnO on the Stability of Nonfullerene Acceptors and its Mitigation by SnO2 for Nonfullerene Organic Solar Cells. *Mater. Horiz.* 6 (7), 1438–1443. doi:10.1039/c9mh00379g

Kini, G. P., Jeon, S. J., and Moon, D. K. (2021). Latest Progress on Photoabsorbent Materials for Multifunctional Semitransparent Organic Solar Cells. *Adv. Funct. Mater.* 31 (15), 2007931. doi:10.1002/adfm.202007931

Krishna, A., Sabba, D., Li, H., Yin, J., Boix, P. P., Soci, C., et al. (2014). Novel Hole Transporting Materials Based on Triptycene Core for High Efficiency Mesoscopic Perovskite Solar Cells. *Chem. Sci.* 5 (7), 2702–2709. doi:10.1039/c4sc00814f

Kyeong, M., Lee, J., Daboczi, M., Stewart, K., Yao, H., Cha, H., et al. (2021). Organic Cathode Interfacial Materials for Non-fullerene Organic Solar Cells. *J. Mater. Chem. A.* 9 (23), 13506–13514. doi:10.1039/d1ta01609a

Li, S., Zhan, L., Liu, F., Ren, J., Shi, M., Li, C.-Z., et al. (2018). An Unfused-Core-Based Nonfullerene Acceptor Enables High-Efficiency Organic Solar Cells with Excellent Morphological Stability at High Temperatures. *Adv. Mater.* 30 (6), 1705208. doi:10.1002/adma.201705208

Li, W., Liu, D., and Wang, T. (2021a). Stability of Non-Fullerene Electron Acceptors and Their Photovoltaic Devices. *Adv. Funct. Mater.* 31 (41), 2104552. doi:10.1002/adfm.202104552

Li, Y., Huang, X., Ding, K., Sheriff, H. K. M., Jr., Ye, L., Liu, H., et al. (2021b). Non-Fullerene Acceptor Organic Photovoltaics with Intrinsic Operational Lifetimes over 30 Years. *Nat. Commun.* 12 (1), 5419. doi:10.1038/s41467-021-25718-w

Li, Z. a., Chueh, C.-C., and Jen, A. K.-Y. (2019). Recent Advances in Molecular Design of Functional Conjugated Polymers for High-Performance Polymer Solar Cells. *Prog. Polym. Sci.* 99, 101175. doi:10.1016/j.progpolymsci.2019.101175

Lin, Y., Wang, J., Zhang, Z.-G., Bai, H., Li, Y., Zhu, D., et al. (2015). An Electron Acceptor Challenging Fullerenes for Efficient Polymer Solar Cells. *Adv. Mater.* 27 (7), 1170–1174. doi:10.1002/adma.201404317

Liu, B., Han, Y., Li, Z., Gu, H., Yan, L., Lin, Y., et al. (2020a). Visible Light-Induced Degradation of Inverted Polymer:Nonfullerene Acceptor Solar Cells: Initiated by the Light Absorption of ZnO Layer. *Sol. RRL* 5 (1), 2000638. doi:10.1002/solr.202000638

Liu, H., Li, Y., Xu, S., Zhou, Y., and Li, Z. a. (2021a). Emerging Chemistry in Enhancing the Chemical and Photochemical Stabilities of Fused-Ring Electron Acceptors in Organic Solar Cells. *Adv. Funct. Mater.* 31 (50), 2106735. doi:10.1002/adfm.202106735

Liu, H., Wang, W., Zhou, Y., and Li, Z. a. (2021b). A Ring-Locking Strategy to Enhance the Chemical and Photochemical Stability of A-D-A-type Nonfullerene Acceptors. *J. Mater. Chem. A.* 9 (2), 1080–1088. doi:10.1039/d0ta09924d

Liu, H., Yu, M. H., Lee, C. C., Yu, X., Li, Y., Zhu, Z., et al. (2021c). Technical Challenges and Perspectives for the Commercialization of Solution-Processable Solar Cells. *Adv. Mater. Technol.* 6 (6), 2000960. doi:10.1002/admt.202000960

Liu, W., Xu, X., Yuan, J., Leclerc, M., Zou, Y., and Li, Y. (2021d). Low-Bandgap Non-fullerene Acceptors Enabling High-Performance Organic Solar Cells. *ACS Energ. Lett.* 6 (2), 598–608. doi:10.1021/acsenergylett.0c02384

Liu, X., Wei, Y., Zhang, X., Qin, L., Wei, Z., and Huang, H. (2020b). An A-D-A′-D-A Type Unfused Nonfullerene Acceptor for Organic Solar Cells with Approaching 14% Efficiency. *Sci. China Chem.* 64 (2), 228–231. doi:10.1007/s11426-020-9868-8

Liu, Z.-X., Yu, Z.-P., Shen, Z., He, C., Lau, T.-K., Chen, Z., et al. (2021e). Molecular Insights of Exceptionally Photostable Electron Acceptors for Organic Photovoltaics. *Nat. Commun.* 12 (1), 3049. doi:10.1038/s41467-021-23389-1

Lu, X., Cao, L., Du, X., Lin, H., Zheng, C., Chen, Z., et al. (2021). Hydrogen-Bond-Induced High Performance Semitransparent Ternary Organic Solar Cells with 14% Efficiency and Enhanced Stability. *Adv. Opt. Mater.* 9 (12), 2100064. doi:10.1002/adom.202100064

Luo, D., Li, L., Shi, Y., Zhang, J., Wang, K., Guo, X., et al. (2021). Electron-Deficient Diketone Unit Engineering for Non-fused Ring Acceptors Enabling over 13% Efficiency in Organic Solar Cells. *J. Mater. Chem. A.* 9 (26), 14948–14957. doi:10.1039/d1ta03643b

Ma, L., Zhang, S., Zhu, J., Wang, J., Ren, J., Zhang, J., et al. (2021). Completely Non-fused Electron Acceptor with 3D-Interpenetrated Crystalline Structure Enables Efficient and Stable Organic Solar Cell. *Nat. Commun.* 12 (1), 5093. doi:10.1038/s41467-021-25394-w

Mandal, S. K., Itkis, M. E., Chi, X., Samanta, S., Lidsky, D., Reed, R. W., et al. (2005). New Family of Aminophenalenyl-Based Neutral Radical Molecular Conductors: Synthesis, Structure, and Solid State Properties. *J. Am. Chem. Soc.* 127 (22), 8185–8196. doi:10.1021/ja0502728

Morita, Y., Nishida, S., Murata, T., Moriguchi, M., Ueda, A., Satoh, M., et al. (2011). Organic Tailored Batteries Materials Using Stable Open-Shell Molecules with Degenerate Frontier Orbitals. *Nat. Mater* 10 (12), 947–951. doi:10.1038/nmat3142

Ospina, F., Ramirez, A., Cano, M., Hidalgo, W., Schneider, B., and Otálvaro, F. (2017). Synthesis of Positional Isomeric Phenylphenalenones. *J. Org. Chem.* 82 (7), 3873–3879. doi:10.1021/acs.joc.6b02985

Park, S., and Son, H. J. (2019). Intrinsic Photo-Degradation and Mechanism of Polymer Solar Cells: The Crucial Role of Non-fullerene Acceptors. *J. Mater. Chem. A.* 7 (45), 25830–25837. doi:10.1039/c9ta07417a

Prasetio, A., Jahandar, M., Kim, S., Heo, J., Kim, Y. H., and Lim, D. C. (2021). Mitigating the Undesirable Chemical Reaction between Organic Molecules for Highly Efficient Flexible Organic Photovoltaics. *Adv. Sci.* 8 (14), 2100865. doi:10.1002/advs.202100865

Qin, F., Wang, W., Sun, L., Jiang, X., Hu, L., Xiong, S., et al. (2020). Robust Metal Ion-Chelated Polymer Interfacial Layer for Ultraflexible Non-fullerene Organic Solar Cells. *Nat. Commun.* 11 (1), 4508. doi:10.1038/s41467-020-18373-0

Qin, M., Cheng, P., Mai, J., Lau, T.-K., Zhang, Q., Wang, J., et al. (2017). Enhancing Efficiency and Stability of Organic Solar Cells by UV Absorbent. *Sol. RRL* 1 (12), 1700148. doi:10.1002/solr.201700148

Raman, K. V., Kamerbeek, A. M., Mukherjee, A., Atodiresei, N., Sen, T. K., Lazić, P., et al. (2013). Interface-Engineered Templates for Molecular Spin Memory Devices. *Nature* 493 (7433), 509–513. doi:10.1038/nature11719

Ren, H., Ma, Y., Liu, H. M., Chen, J. D., Zhang, Y. F., Hou, H. Y., et al. (2021). Absorption Spectrum-Compensating Configuration Reduces the Energy Loss of Nonfullerene Organic Solar Cells. *Adv. Funct. Mater.*, 2109735. doi:10.1002/adfm.202109735

Wang, J., Zheng, Z., Zu, Y., Wang, Y., Liu, X., Zhang, S., et al. (2021). A Tandem Organic Photovoltaic Cell with 19.6% Efficiency Enabled by Light Distribution Control. *Adv. Mater.* 33 (39), e2102787. doi:10.1002/adma.202102787

Wen, T. J., Liu, Z. X., Chen, Z., Zhou, J., Shen, Z., Xiao, Y., et al. (2021). Simple Non-Fused Electron Acceptors Leading to Efficient Organic Photovoltaics. *Angew. Chem. Int. Ed.* 60 (23), 12964–12970. doi:10.1002/anie.202101867

Xie, L., Song, W., Ge, J., Tang, B., Zhang, X., Wu, T., et al. (2021). Recent Progress of Organic Photovoltaics for Indoor Energy Harvesting. *Nano Energy* 82, 105770. doi:10.1016/j.nanoen.2021.105770

Xiong, S., Hu, L., Hu, L., Sun, L., Qin, F., Liu, X., et al. (2019). 12.5% Flexible Nonfullerene Solar Cells by Passivating the Chemical Interaction between the Active Layer and Polymer Interfacial Layer. *Adv. Mater.* 31 (22), e1806616. doi:10.1002/adma.201806616

Yassin, A., Rousseau, T., Leriche, P., Cravino, A., and Roncali, J. (2011). Evaluation of Bis-Dicyanovinyl Short-Chain Conjugated Systems as Donor Materials for Organic Solar Cells. *Solar Energ. Mater. Solar Cell* 95 (2), 462–468. doi:10.1016/j.solmat.2010.08.032

Yin, Y., Zhan, L., Liu, M., Yang, C., Guo, F., Liu, Y., et al. (2021). Boosting Photovoltaic Performance of Ternary Organic Solar Cells by Integrating A Multi-Functional Guest Acceptor. *Nano Energy* 90, 106538. doi:10.1016/j.nanoen.2021.106538

Yu, Z.-P., Liu, Z.-X., Chen, F.-X., Qin, R., Lau, T.-K., Yin, J.-L., et al. (2019). Simple Non-fused Electron Acceptors for Efficient and Stable Organic Solar Cells. *Nat. Commun.* 10 (1), 2152. doi:10.1038/s41467-019-10098-z

Zeng, W., Zhou, X., Du, B., Hu, L., Xie, C., Wang, W., et al. (2021). Minimizing the Thickness of Ethoxylated Polyethylenimine to Produce Stable Low-Work Function Interface for Nonfullerene Organic Solar Cells. *Adv. Energ. Sustain Res* 2 (5), 2000094. doi:10.1002/aesr.202000094

Zheng, Z., He, E., Wang, J., Qin, Z., Niu, T., Guo, F., et al. (2021). Revealing the Role of Solvent Additives in Morphology and Energy Loss in Benzodifuran Polymer-Based Non-fullerene Organic Solar Cells. *J. Mater. Chem. A.* 9 (46), 26105–26112. doi:10.1039/d1ta08893a

Zhou, Y., Li, M., Lu, H., Jin, H., Wang, X., Zhang, Y., et al. (2021). High-Efficiency Organic Solar Cells Based on a Low-Cost Fully Non-Fused Electron Acceptor. *Adv. Funct. Mater.* 31 (27), 2101742. doi:10.1002/adfm.202101742

Zhu, X., Liu, S., Yue, Q., Liu, W., Sun, S., and Xu, S. (2021). Design of All-Fused-Ring Electron Acceptors with High Thermal, Chemical, and Photochemical Stability for Organic Photovoltaics. *CCS Chem.* 3 (6), 1070–1080. doi:10.31635/ccschem.021.202100956

Conflict of Interest: The authors declare that the research was conducted in the absence of any commercial or financial relationships that could be construed as a potential conflict of interest.

Publisher's Note: All claims expressed in this article are solely those of the authors and do not necessarily represent those of their affiliated organizations, or those of the publisher, the editors, and the reviewers. Any product that may be evaluated in this article, or claim that may be made by its manufacturer, is not guaranteed or endorsed by the publisher.

Copyright © 2022 Liu, Hsieh, He, Chueh and Li. This is an open-access article distributed under the terms of the Creative Commons Attribution License (CC BY). The use, distribution or reproduction in other forums is permitted, provided the original author(s) and the copyright owner(s) are credited and that the original publication in this journal is cited, in accordance with accepted academic practice. No use, distribution or reproduction is permitted which does not comply with these terms.